

Magnetic structure of the square cupola compound Ba(TiO)Cu₄(PO₄)₄Riho Rästa¹,¹ Ivo Heinmaa,¹ Kenta Kimura,² Tsuyoshi Kimura,² and Raivo Stern^{1,*}¹National Institute of Chemical Physics and Biophysics, Akadeemia tee 23, 12618 Tallinn, Estonia²Department of Advanced Materials Science, University of Tokyo, Kashiwa, Chiba 277-8561, Japan

(Received 20 November 2019; accepted 22 January 2020; published 12 February 2020; corrected 12 May 2020)

The magnetic structure of the antiferromagnetic square cupola compound Ba(TiO)Cu₄(PO₄)₄ with the tetragonal structure is studied with ³¹P and ^{63,65}Cu nuclear magnetic resonance techniques. The ³¹P magnetic hyperfine shift K shows a clear splitting at the Néel temperature $T_N = 9.5$ K, where the resonance breaks down into two lines when an external magnetic field is oriented along the c axis and into four lines when the field is along the a axis. In the paramagnetic region $K(T)$ follows the temperature dependence of the magnetic susceptibility $\chi(T)$. From the K vs χ plot we determined nearly equal hyperfine field values $H_{\text{hf}}^a = 765$ mT/ μ_B and $H_{\text{hf}}^c = 740$ mT/ μ_B for the magnetic field oriented along a and c , respectively. From the rotation of the single crystal in the external magnetic field we determined eight different orientations of the K tensor in the paramagnetic region. In the antiferromagnetic state at $T = 6$ K, the rotation of the single crystal shows at phosphorus eight different orientations of the local field $B_{\text{int}} = 35.6$ mT. The NMR spectrum of copper at zero external field shows local field at copper nucleus $B_{\text{loc}} = 14.77$ T, directed perpendicular to the plane of the CuO₄ plaquette, confirming a previously determined quadrupolar configuration of magnetic moments $\Gamma_3(2)$ [K. Kimura *et al.*, *Nat. Commun.* **7**, 13039 (2016); P. Babkevich *et al.*, *Phys. Rev. B* **96**, 214436 (2017)].

DOI: [10.1103/PhysRevB.101.054417](https://doi.org/10.1103/PhysRevB.101.054417)**I. INTRODUCTION**

An interesting novel class of compounds, $AE(\text{TiO})\text{Cu}_4(\text{PO}_4)_4$ ($AETCPO$; $AE = \text{Ba}, \text{Sr}, \text{or Pb}$), was recently synthesized [1,2]. The structure of $AETCPO$ is tetragonal with the space group $P4_212$ and consists of the layers of up and down square cupolas of Cu₄O₁₂ (Fig. 1). Each square cupola is made of four corner-sharing CuO₄ plaquettes. The layers are separated by AE ions and TiO₅ pyramids. These compounds undergo an antiferromagnetic (AF) transition at low temperatures. For example, Ba(TiO)Cu₄(PO₄)₄ (BaTCPO) exhibits an AF ordered state at temperatures below the Néel temperature $T_N = 9.5$ K. Below T_N the arrangement of magnetic moments of copper atoms shows an antiferroic quadrupolar order. Because of the antiferroic order, BaTCPO does not exhibit a magnetoelectric effect where an electric (magnetic) field causes magnetization (electric polarization). Instead, this compound exhibits a remarkable magnetodielectric effect. Sr(TiO)Cu₄(PO₄)₄ (SrTCPO) also shows similar magnetic and magnetodielectric properties below $T_N = 6.2$ K [3], while Pb(TiO)Cu₄(PO₄)₄ (PbTCPO) exhibits a ferroic quadrupolar order resulting in a linear magnetoelectric effect below $T_N = 6.5$ K [4,5].

The magnetic structure of BaTCPO was carefully studied by neutron scattering experiments [1]. These studies yielded

two possible arrangements of the spins: one, denoted $\Gamma_3(1)$, where the moments are confined approximately in the CuO₄ planes and one, $\Gamma_3(2)$, where the moments are approximately perpendicular to the CuO₄ planes forming two-in-two-out-type structure (Fig. 1). The latter arrangement had smaller R factor, thus being the most likely arrangement. Later, Babkevich *et al.* [6] confirmed the two possible structures using spherical neutron polarimetry, inclining by a discernible, albeit small, advantage towards the $\Gamma_3(2)$ spin structure.

In the present report we will use ³¹P and ^{63,65}Cu NMR techniques to study the local magnetic fields in a single crystal of BaTCPO. Phosphorus ions in PO₄ tetrahedrons see four copper atoms in two cupolas as next-nearest neighbors. Therefore, the local field at phosphorus is definitely influenced by the magnetic arrangement of copper atoms. Previous NMR studies of SrTCPO [7] and BaTCPO [8] used powder samples from which such detailed information about the magnetic structure is difficult to get. In addition, the ^{63,65}Cu NMR provides the on-site local field in the ordered state.

II. EXPERIMENTAL DETAILS

Single crystals of Ba(TiO)Cu₄(PO₄)₄ were grown with the flux method by Kimura *et al.* [2,9]. The sample crystal used in the experiments was $1.9 \times 2.0 \times 3.9$ mm³ and weighed 61.84 mg. Magnetic susceptibility was measured using the vibrating-sample magnetometer option of the 14T-PPMS (Quantum Design). Single-crystal ³¹P NMR measurements were conducted using the spectrometer MAGRes2000 attached to a $B = 4.7$ T superconducting magnet (resonance frequency of 80.97 MHz). A He-flow cryostat (Janis Research Inc.) allowed measurements in the temperature range of 4.5 to 300 K. The NMR probe was homemade and had a

*raivo.stern@kbfi.ee

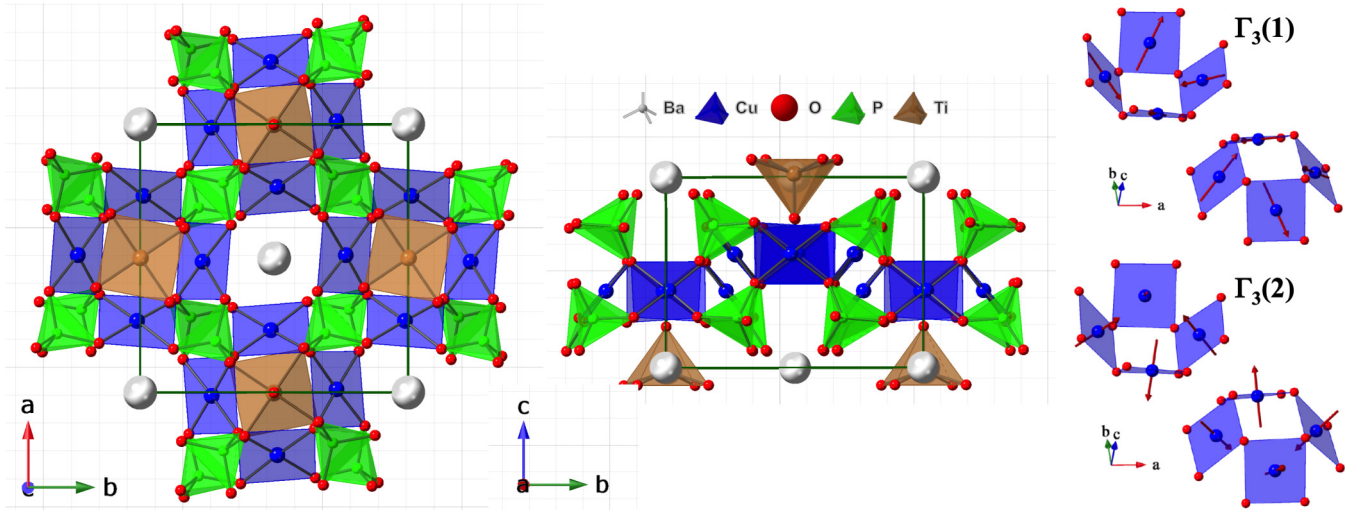


FIG. 1. Description of the BTCPO unit cell with up and down Cu_4O_{12} square cupolas (blue), PO_4 tetrahedrons (green), and TiO_5 pyramids (brown), with Ba ions shown as large gray spheres along the c (left panel) and a (middle panel) axes. Two possible arrangements of spins $\Gamma_3(1)$ and $\Gamma_3(2)$ (right panel).

single-axis goniometer. Lake Shore Cernox calibrated sensors and a model 332 temperature controller were used for temperature regulation. Spin-lattice relaxation T_1 was measured using the inversion-recovery method. The magic-angle spinning (MAS) room-temperature spectrum was recorded using the powder sample and a home-built probe with a 1.8-mm-o.d. rotor spinning at 25 kHz. The magnetic shifts are given relative to the resonance of H_3PO_4 . $^{63,65}\text{Cu}$ NMR on the powder sample was performed in zero applied field using a liquid-He bath. Powder NMR spectra were recorded using a commercial Avance II spectrometer (Bruker).

III. RESULTS AND ANALYSIS

A. Magnetization

The temperature dependence of magnetic susceptibility was measured with the applied magnetic field $B = 4.7$ T along the [001] and [100] directions, as shown in Fig. 2. At temperature region $T^{\text{max}} \approx 17$ K there is a broad maximum of the χ vs T curve, which indicates the onset of short-range order.

At high temperature $\chi(T)$ followed the Curie-Weiss law:

$$\chi(T) = \chi_0 + \frac{C}{T - \theta_{\text{CW}}}. \quad (1)$$

Here, χ_0 is temperature-independent susceptibility. At $T > 100$ K the fitting gives the following parameters: for the magnetic field along the [001] direction, $\chi_0 = -7.3(4) \times 10^{-5} \text{ cm}^3/\text{mole}$ per Cu, $C = 0.460(1) \text{ cm}^3 \text{ K}/\text{mole}$ Cu, $\theta_{\text{CW}} = -29.0(4)$ K, and for the field along the [100] direction, $\chi_0 = -3.5(2) \times 10^{-5} \text{ cm}^3/\text{mole}$ Cu, $C = 0.454(7) \times 10^{-4} \text{ cm}^3 \text{ K}/\text{mole}$ Cu, and $\theta_{\text{CW}} = -29.3(2)$ K. From the Curie constant one gets the effective copper magnetic moment as $\mu_{\text{eff}} = \sqrt{3k_B C/N_A}$, where k_B is the Boltzmann factor and N_A is Avogadro's number. We get $\mu_{\text{eff}} = 1.920\mu_B$ and $1.911\mu_B$ for the [001] and [100] directions, respectively. Here, μ_B is the Bohr magneton. Using $g = \sqrt{S(S+1)}\mu_{\text{eff}}$, we get almost equal Landé g factor values as $g = 2.22$ and $g = 2.20$

for [001] and [100], respectively, which are common for Cu^{2+} ions.

Here, we note that in regular, collinear antiferromagnets χ vanishes in the direction where the local magnetic moments are aligned parallel or antiparallel to an external magnetic field and stays constant in the directions where the external field is perpendicular to the local magnetic moments [10]. Thus, the local moments here may prefer the [001] direction, but the nonvanishing χ could also just be a signature of the noncollinear order.

B. ^{31}P Knight shift

The temperature dependence of the ^{31}P Knight shift is presented in Fig. 3. Above the Néel temperature $T_N = 9.5$ K,

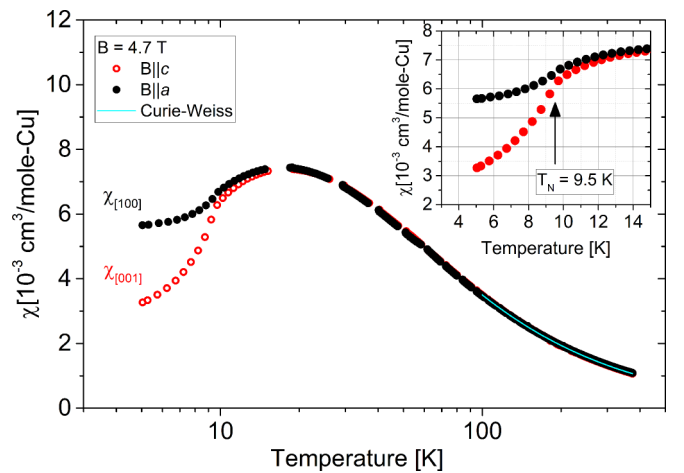


FIG. 2. Temperature dependence of magnetic susceptibility $\chi(T)$ in an applied magnetic field $B = 4.7$ T, measured in two different directions: $B \parallel [100]$ (black solid circles) and $B \parallel [001]$ (red open circles). The cyan line represents the Curie-Weiss fit. The inset shows the detailed behavior of susceptibilities below $T_N = 9.5$ K.

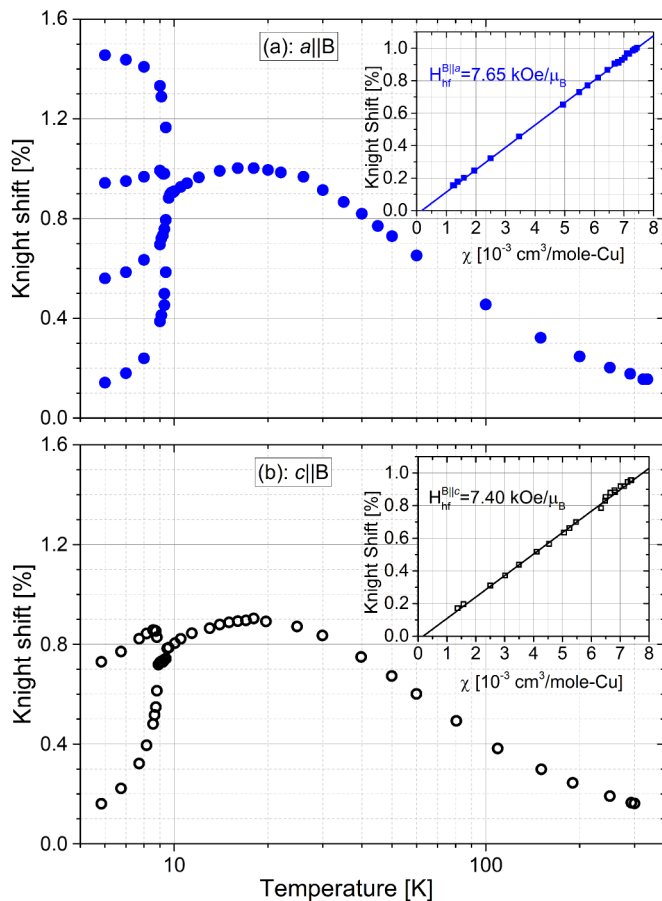


FIG. 3. Temperature dependence of the ^{31}P Knight shift as measured when the single crystal is oriented (a) with the a axis parallel to the external field B (blue dots) and (b) with the c axis parallel to B (open circles). The insets show the Clogston-Jaccarino plots, giving values quite close to the hyperfine field in both the directions.

the Knight shift $K(T)$ follows perfectly the magnetic susceptibility curve $\chi(T)$, as given [11] by Eq. (2):

$$K(T) = K_0 + \frac{H_{\text{hf}}}{N_A \mu_B} \chi. \quad (2)$$

Here, K_0 is the temperature-independent shift, the chemical shift, and H_{hf} is the hyperfine coupling constant. From the K vs χ plots (insets of Fig. 3) we found the hyperfine field values are $H_{\text{hf}} = 7.65(5)$ kOe/ μ_B for the $a||B$ direction and a slightly smaller value, $H_{\text{hf}} = 7.40(5)$ kOe/ μ_B , for direction $c||B$.

Below T_N , due to the onset of local magnetic fields, the resonance line splits into four lines in the orientation $a||B$ and into two lines when the crystal is oriented with $c||B$. Following the approach given in Ref. [7], we will estimate the critical order parameter β of the phase transition from the growth of the internal field B_{int} in the vicinity of the ordering temperature. As a measure of the internal field we use the frequency difference between the most shifted resonance lines instead of the internal ones, which is proportional to the internal field by the gyromagnetic ratio $^{31}\gamma/2\pi = 17.237$ MHz/T. The temperature dependences of the frequency differences in the two orientations of the single crystal are given in Fig. 4.

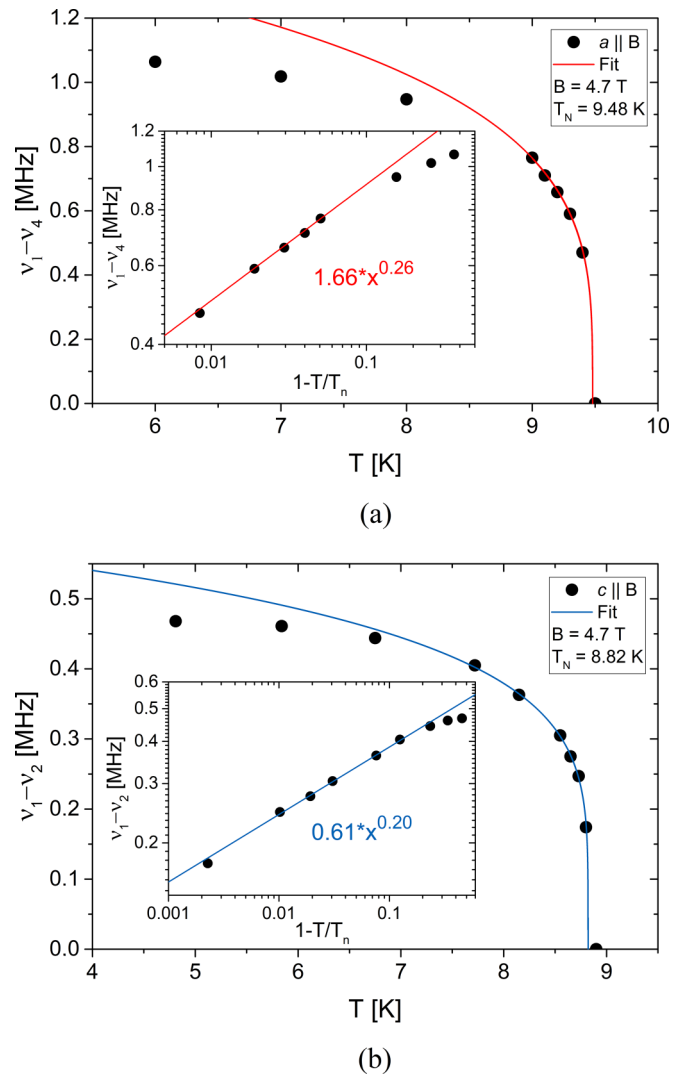


FIG. 4. Temperature development of the splitting of the resonance lines below the ordering temperature in the orientation $a||B$ (top panel) and $c||B$ (bottom panel). The solid lines are fits by Eq. (3).

The temperature dependence of the frequency difference is fitted by the formula

$$\Delta F(T) = \Delta F_0 \left(1 - \frac{T}{T_n}\right)^\beta. \quad (3)$$

The best fit was obtained with $T_N = 9.48$ K, $\beta = 0.26$ for the orientation $a||B$ and $T_N = 8.82$ K, $\beta = 0.20$ for $c||B$. The critical exponent β values, if compared to some theoretical values (as given, e.g., in Ref. [12]), indicate that the ordering scheme is the closest to the two-dimensional XY case.

C. ^{31}P NMR of powder sample

Before starting ^{31}P analysis of the single crystal we recorded the spectrum of a powder sample. Figure 5(a) shows the ^{31}P NMR spectrum recorded with magic-angle spinning [13] of the sample. The spectrum shows a single sharp line at the isotropic magnetic shift. The spectrum of a static sample [Fig. 5(b)] shows a typical powder line shape with

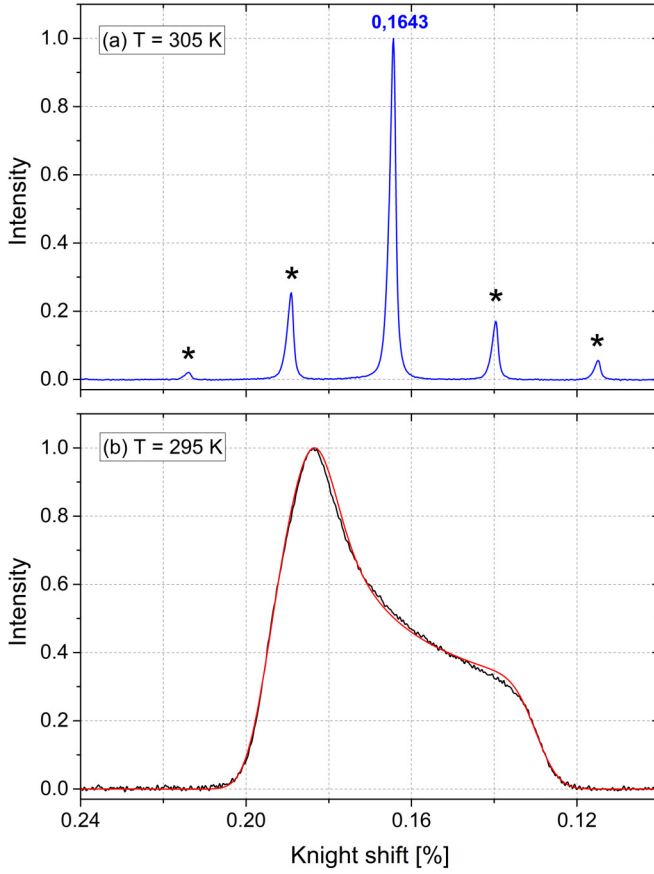


FIG. 5. (a) ^{31}P MAS NMR of the BaTCPO powder sample at $T = 305$ K with a spinning frequency $\nu = 25$ kHz. The NMR spectrum of the rotating sample consists of a center band at isotropic Knight shift $K_{\text{iso}} = 0.1643\%$ and of a number of spinning sidebands denoted by asterisks at multiples of the spinning frequency from the center band. (b) ^{31}P NMR of a static powder sample at slightly lower temperature $T = 295$ K. The red line is a fit to the powder line with the eigenvalues of the nearly axially symmetric Knight shift tensor: $K_{11} = 0.1952\%$, $K_{22} = 0.1832\%$, $K_{33} = 0.1298\%$.

singularities at the principal values of the Knight shift tensor:

$$K_{PAS} = \begin{pmatrix} 1 + K_{11} & 0 & 0 \\ 0 & 1 + K_{22} & 0 \\ 0 & 0 & 1 + K_{33} \end{pmatrix}, \quad (4)$$

with $K_{11} = 0.1952\%$, $K_{22} = 0.1832\%$, $K_{33} = 0.1298\%$. These values give us the reference for the interpretation of the rotation patterns of the single crystal.

D. Orientation of the ^{31}P Knight shift tensor

Determination of the tensor orientation in a single crystal is not a very easy task [14]. For that, in the general case, one needs to record resonance frequencies rotating the sample around three different axes. Depending on symmetry or with some principal values of the shift tensor predetermined, the number of necessary rotation patterns may be smaller. After obtaining those rotation patterns, one needs to find the unitary transformation that will transform the principal-axis system (PAS) into the crystal frame. As usual, the Hamiltonian of

the spin- $\frac{1}{2}$ nucleus consists of the Zeeman and Knight shift interaction,

$$\mathcal{H} = \mathcal{H}_Z + \mathcal{H}_K = \gamma \mathbf{H}_0 \cdot \mathbf{K} \cdot \mathbf{I}, \quad (5)$$

where $\mathbf{I} = (I_x, I_y, I_z)^T$, $\mathbf{H}_0 = (0, 0, H_0)$, and I_x, I_y, I_z are Pauli matrices:

$$I_x = \frac{\hbar}{2} \begin{pmatrix} 0 & 1 \\ 1 & 0 \end{pmatrix}, \quad I_y = \frac{\hbar}{2} \begin{pmatrix} 0 & i \\ -i & 0 \end{pmatrix}, \quad I_z = \frac{\hbar}{2} \begin{pmatrix} 1 & 0 \\ 0 & -1 \end{pmatrix}. \quad (6)$$

Three successive rotations, each characterized by three Euler angles, transform the Hamiltonian from the PAS into the laboratory frame:

$$K_{PAS} \xrightarrow{R_p(a_1, a_2, a_3)} K^* \xrightarrow{R_i(b_1, b_2, b_3)} K_g \xrightarrow{R_g(c_1, c_2, c_3)} K \xrightarrow{(x, y, z)}$$

There are four frames of reference: PAS with a diagonal tensor (K_{PAS}), the crystal frame (K^*), the goniometer frame (K_g), and the laboratory frame (K). The transformations between them are R_p, R_i, R_g with the corresponding Euler angles. We used the conventional Euler ZYZ rotation of the Hamiltonian [15].

In BaTCPO there are eight different positions of the phosphorus ions in the unit cell, each giving the resonance corresponding to different transformations R_p . The rotation patterns around the c and a axes at temperatures $T = 295$ K and $T = 18$ K are shown in Fig. 6. The angles b_1, b_2, b_3 and c_1, c_2, c_3 are unique for each experiment; a_1, a_2, a_3 are eight desired sets of the Euler angles transforming the tensor in PAS to the crystal frame for each phosphorus site. It turns out that the principal axis K_{33} of the Knight shift tensor is tilted by 45° from the crystal c axis. Schematics of the Knight tensor's eight orientations are presented in Fig. 7.

E. Spin-lattice relaxation results

Spin-lattice relaxation T_1 was measured with an inversion-recovery pulse sequence at magnetic fields along the [001] and [100] directions (Fig. 8). The magnetization recovery was exponential throughout all the measurements:

$$M(\tau) = M_0[1 - A \exp(-\tau/T_1)], \quad (7)$$

where $M(\tau)$ is the magnetization at delay τ after inversion, M_0 is the equilibrium magnetization, and $A \leq 2$ is a constant depending on the accuracy of the inversion.

The relaxation rate at $T > 60$ K is almost constant, which is typical for a paramagnetic material, where the relaxation is caused by the fluctuation of the magnetic moments. Before the phase transition at T_N , a sharp spike occurs in the relaxation speed which is connected to the rapid slowing of the fluctuations. Below T_N , relaxation speed decreases sharply proportional to T^7 . In the case of $c \parallel \mathbf{B}$, the relaxation rate seems to have a discontinuity in close vicinity to T_N . Here, we note that $1/T_1 \propto T^7$ was also observed for SrTCPO [7].

In the paramagnetic, high-temperature region we try to use Moriya's theory of relaxation [16]:

$$\frac{1}{T_1} = \frac{2\gamma_N^2 \sqrt{2\pi} S(S+1)}{3\omega_{EZ'}} H_{hf}^2, \quad (8)$$

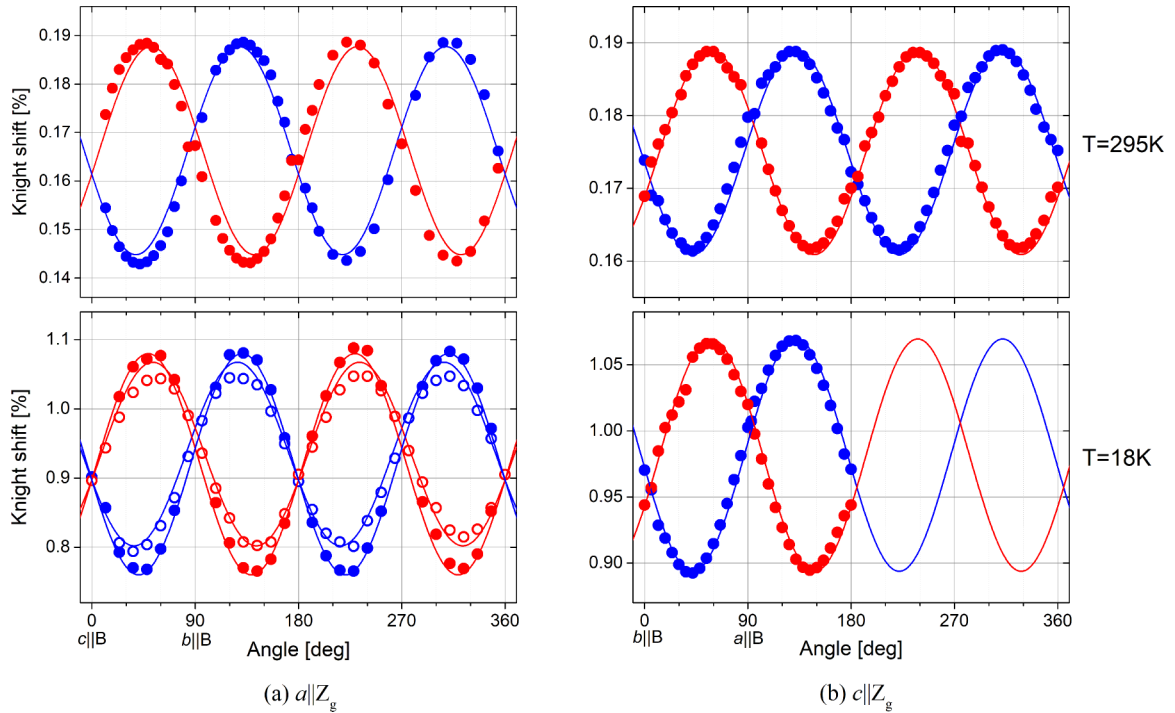


FIG. 6. ^{31}P NMR resonance frequencies by rotating the BaTCPO single crystal around the (a) a and (b) c axes at $T = 295$ K (top panels) and $T = 18$ K (bottom panels). The solid lines correspond to the angle dependences according to the parameters given in Table I. Due to symmetry, eight different sites in the unit cell contribute to only two different rotation patterns. The red lines correspond to sites 1, 3, 6, and 7 (see Table I) in (a) and to sites 2, 3, 6, and 8 in (b); the rest of the sites are given by the blue lines.

where γ_N is the nuclear gyromagnetic ratio, S is the nuclear spin, H_{hf} is the total hyperfine field as in Eq. (2), $z' = 4$ is the number of nearest Cu^{2+} neighbors for the ^{31}P nucleus, the 2 in numerator stands for summing the two equal projections of hyperfine field perpendicular to the magnetic field, and $\omega_E = (|Jk_B/\hbar|\sqrt{2zS(S+1)/3})$ is the Heisenberg exchange frequency (in rad/s), where $z = 2$ is the number of Cu^{2+} ions that are nearest neighbors to copper, $S = 1/2$ is the electronic spin, and J is the exchange interaction.

With a hyperfine field value of $H_{hf} = 7.650$ kOe/ μ_B , a relaxation rate for the paramagnetic, high-temperature region $\frac{1}{T_1} = 1410$ s $^{-1}$, and an exchange frequency of $\omega_E = 1.5 \times 10^{12}$ rad/s, we get an estimate for the exchange interaction inside the square cupola $J/k_B = 12$ K. This value is about 3 times smaller than the previous result for BaTCPO of $J = 3.0$ meV = 34.8 K [1] or density functional theory calculated $J/k_B = 27.9$ K for SrTCPO [7], while it is not so far from the experimentally determined $J/k_B = 16.3$ K for SrTCPO [7].

F. Local magnetic structure in the ordered state

The resonance frequencies by rotation of the single crystal around [001] and [100] at $T = 6$ K are given in Fig. 9. The results are coherent with the Knight shift temperature dependence (Fig. 3). Once the magnetic field is turned around the c axis, one can see that when $a||B$, there are four different magnetic field projections in the antiferromagnetic region, as given in Fig. 3(a). When the crystal is oriented $c||B$, there are two different local field projections to the external field direction, as given in Fig. 3(b). Rotating the sample around c and

a gives eight different rotation patterns for eight phosphorus ions in the unit cell. Each rotation pattern can be described by the equation

$$F = K + L \cos(\alpha - \alpha_1) + M \cos[2(\alpha - \alpha_2)], \quad (9)$$

where the constant term K is the Larmor frequency plus the average chemical shift; the second term describes the angle dependence of the local field projection to the external field direction. The third term describes the angle dependence of the resonance frequency due to the turning of the chemical shift tensor.

The rotation patterns around the [001] axis show two sets of lines (blue and red). The phase shift within the set is 90° . The red lines are shifted from $b||B$ by $+16^\circ$, while the blue lines are shifted -16° . We assign the blue lines to the phosphorus ions in the “up” cupola and the red lines to the ions in the “down” cupola. The rotation patterns of the crystal around [100] [Fig. 9(b) and Table II] are not so well resolved. Here, the approximation of the frequencies by Eq. (9) is not particularly good. A possible reason might be that the magnetic structure in 4.7-T magnetic field in the $c||B$ direction is not yet well settled at a temperature of 6 K. We found above (see Fig. 4) that the ordering temperature in the direction $c||B$ was $T_N = 8.8$ K, while in the case of $b||B$ we had $T_N = 9.5$ K.

Despite that, one can clearly see the rotation patterns with two different amplitudes as expected for two different local field projections along the b axis. The assignment of the resonances to up and down cupola is not unique. For example, we cannot distinguish the cases where all the local field directions of one cupola have a positive projection to the c axis and

TABLE I. Top: The Euler angles for transforming BaTCPO single-crystal shift tensors from the crystal frame to the laboratory frame. Bottom: The Euler angles for transforming the tensors from PAS to the crystal frame. Tensor components of PAS (K_{11} , K_{22} , K_{33}) are in percentage units of ω_L .

	c_1	c_2	c_3	b_1	b_2	b_3
$T = 295$ K						
$c z_g$	(-12:372)	90	0	85	0	0
$a z_g$	(-12:372)	90	0	0	90	0
$T = 18$ K						
$c z_g$	(-12:372)	90	0	80	0	0
$a z_g$	(-12:372)	90	0	0	90	0
Temperature						
	295 K			18 K		
No.	a_1	a_2	a_3	a_1	a_2	a_3
1	30	45	-45	25	45	-40
2	-30	45	45	-25	45	50
3	30	45	135	25	45	140
4	-30	45	-135	-25	45	-130
5	30	135	45	25	135	50
6	-30	135	-45	-25	135	-40
7	30	135	-135	-25	135	140
8	-30	135	135	25	135	-130
K_{11}	K_{22}	K_{33}				
$T = 295$ K						
0.198	0.185	0.128				
$T = 18$ K						
1.14	1.05	0.67				

the moments of the other cupola have a negative projection from the case where the ions of one cupola have two positive and two negative projections and the field of ions of the other cupola has two negative and two positive projections to the c axis. The assignment in Fig. 9(b) corresponds to the local field configuration as given below in Fig. 11.

The analysis of the data given in Table II can be carried out using the scheme of the local field direction as given in Fig. 10. Three cosine amplitudes L in Table II correspond to the local field projections B_1 , B_2 , and B_3 in Fig. 10. Using the gyromagnetic ratio of ^{31}P $\gamma/2\pi = 17.237$ MHz/T, we find $B_1 = 36$ mT, $B_2 = 32.5$ mT, and $B_3 = 16.8$ mT. The angles $\alpha = \pm 16^\circ$, $\beta = \pm 66^\circ$, and $\gamma = \pm 32^\circ$. It is not difficult to calculate the projections $B_a = 8.9$ mT, $B_b = 31.2$ mT, and $B_c = 14.6$ mT, as well as the module of the internal field $B_{\text{int}} = 35.6$ mT.

As noted above, unique assignment of the resonances to a certain phosphorus in the unit cell is not possible. One possible local field configuration is given in Fig. 11.

The internal field at phosphorus ions consists of two components:

$$B_{\text{int}} = B_{\text{hf}} + B_{\text{dip}}, \quad (10)$$

where B_{hf} is the transferred hyperfine field and B_{dip} is the dipolar field from the magnetic moments of Cu^{2+} ions. We do not have the means to estimate the value of B_{hf} and how well it might be canceled in the AF ordered state, but we can

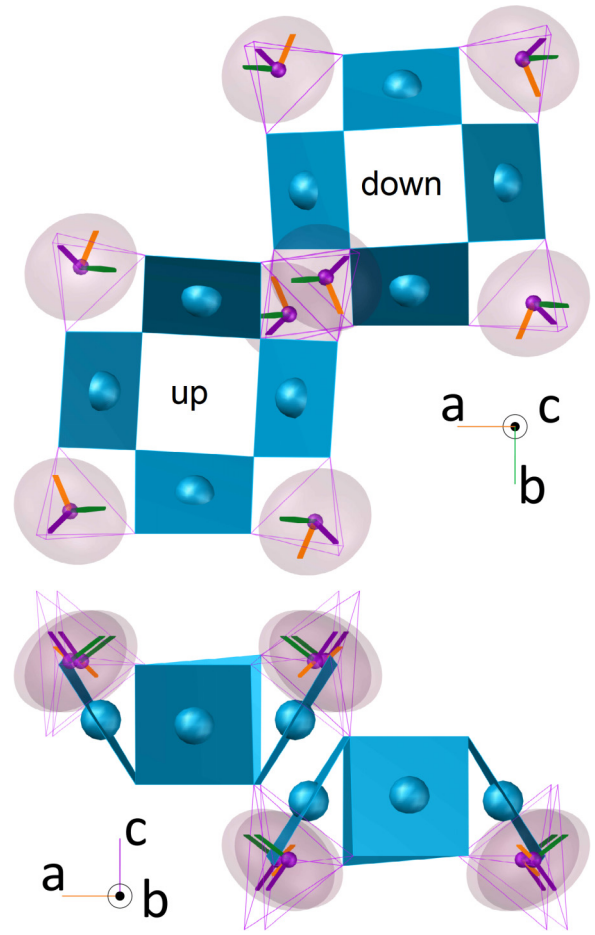


FIG. 7. Orientations of the Knight shift tensor at eight phosphorus locations of the unit cell at temperature $T = 295$ K. The tensors have three principal vectors, green, orange, and dark violet, which correspond to K_{PAS} values K_{11} , K_{22} , and K_{33} , respectively.

estimate the dipolar magnetic field at phosphorus due to Cu^{2+} ions.

We did calculate the dipolar field at each phosphorus ion of the unit cell assuming the *two* magnetic structures proposed

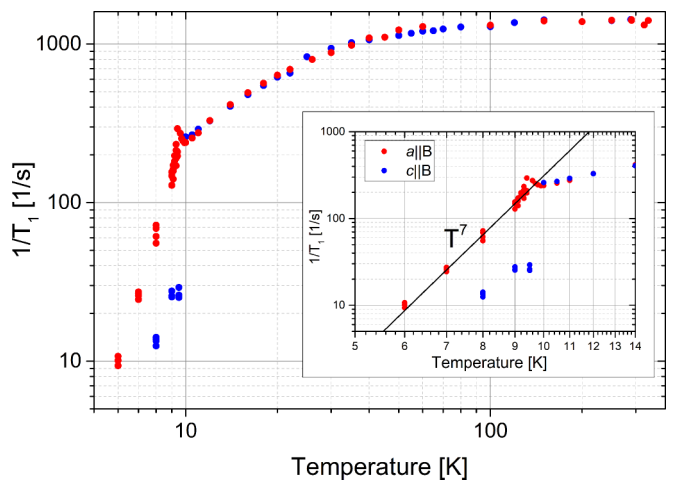


FIG. 8. Temperature dependence of ^{31}P spin-lattice relaxation rate in directions [100] (red dots) and [001] (blue dots). The inset shows that relaxation rate $1/T_1$ is proportional to T^7 below T_N .

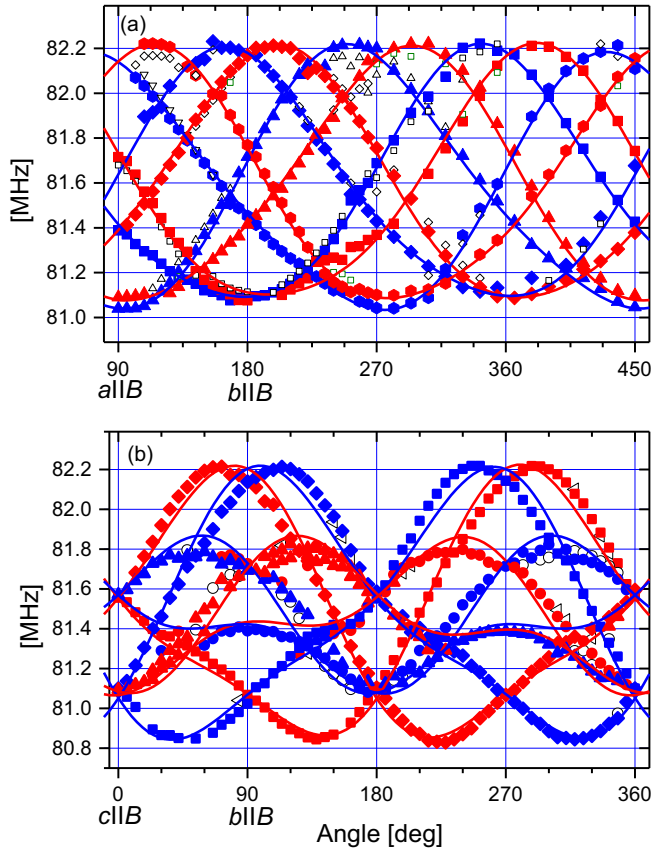


FIG. 9. Rotation patterns of ^{31}P NMR frequencies of the BaTCPO single crystal at temperature $T = 6$ K rotating around (a) [001] and (b) [100]. The lines are approximations with Eq. (9) using data in Table II. The main directions of a crystal, $a\parallel B$, $b\parallel B$, and $c\parallel B$, and $b\parallel B$, are noted on the respective x axes. The blue symbols are assigned to the sites in the up cupola, and the red symbols are assigned to the sites in the down cupola.

in Refs. [1,6] (Table III). In the calculation we summed the dipolar fields from every Cu^{2+} inside a sphere of 50 \AA around a given phosphorus. At that we took into account that the unit cell of the magnetic structure is doubled along the c direction; that is, the magnetic moments of every other layer along the c axis were reversed.

Calculated dipolar field directions at the phosphorus ions are given in Fig. 12. A comparison of the experimental field pattern to the calculated dipolar fields gives a good similarity to the case calculated for the $\Gamma_3(1)$ structure: the calculated dipolar field directions are close to the experimental values in Fig. 11, although the calculated B_c value is relatively small and the total dipolar field is 2.7 times larger than the experimental B_{int} value. A 3 times larger value of the calculated dipolar field compared to the experimentally determined local field was reported earlier for the dipolar field at the Ba site in antiferromagnetic $\text{YBa}_2\text{Cu}_3\text{O}_{6.05}$ [17]. The authors ascribed this controversy to the possible effect of delocalization of the copper d electron. The dipolar field for the $\Gamma_3(2)$ structure is quite different. It is almost confined to the ab plane, with nearly equal B_a and B_b components. Thus, on the one hand,

TABLE II. The fitting parameters K , L , M , α_1 , and α_2 of the rotation patterns according to Eq. (9). The top corresponds to the rotation of the crystal around the c axis [as shown in Fig. 9(a)], and the bottom corresponds to rotation around the a axis [FIG. 9(b)] at temperature $T = 6$ K.

No.	K	L	α_1	M	α_2
Rotation around the c axis					
1	81.59	0.56	347	0.075	155
2	81.59	0.56	20	0.075	25
3	81.58	0.56	80	0.075	50
4	81.59	0.56	110	0.075	125
5	81.59	0.55	170	0.075	155
6	81.595	0.56	198	0.065	30
7	81.59	0.575	258	0.078	50
8	81.60	0.56	288	0.065	130
Rotation around the a axis					
1	81.47	0.62	294	0.17	87
2	81.47	0.62	246	0.17	97
3	81.45	0.29	212	0.17	72
4	81.44	0.29	148	0.17	115
5	81.47	0.62	114	0.17	84
6	81.47	0.62	66	0.17	95
7	81.45	0.29	32	0.17	69
8	81.45	0.29	328	0.17	111

the measured ^{31}P B_{int} seems to be more consistent with the B_{dip} for magnetic structure $\Gamma_3(1)$. On the other hand, a 3 times smaller field at phosphorus may also indicate that a considerable part of the dipolar field is compensated by a transferred hyperfine field B_{hf} from the four nearest-neighbor copper ions [see Eq. (10)]. Unfortunately, the magnitude and direction of this field are difficult to estimate. Instead, we found that the magnitude and direction of the magnetic moment at copper

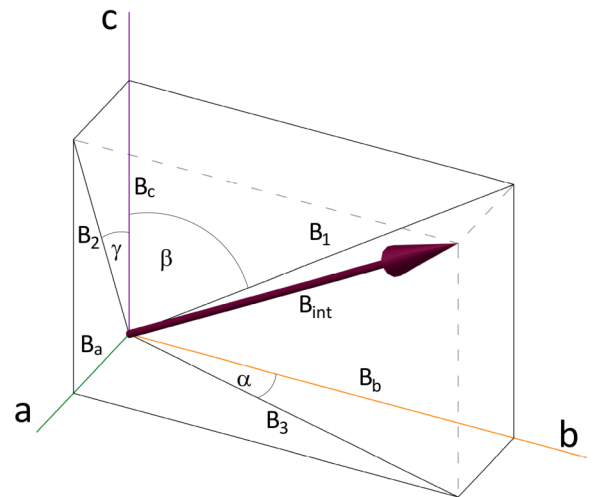


FIG. 10. Scheme of the local field direction on a phosphorus ion in the BaTCPO crystal. B_{int} is the local field; B_a , B_b , and B_c are the projections of B_{int} to the crystal a , b , and c axes, respectively. B_1 , B_2 , and B_3 are the projections of B_{int} to the bc , ac , and bc planes, respectively. The latter amplitudes can be found from the rotation pattern parameters given in Table II.

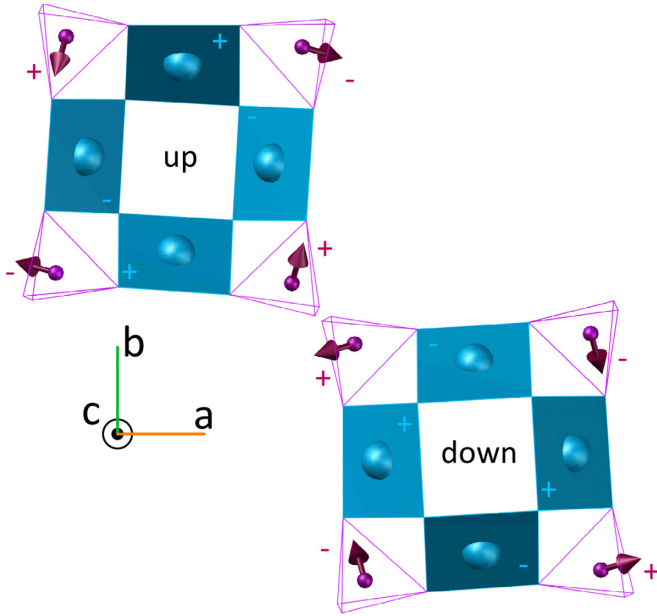


FIG. 11. Possible configuration of induced static magnetic fields at phosphorus ions in the BaTCPO unit cell. Red arrows represent the directions and sizes of the static magnetic fields; plus and minus signs indicate the field direction to the front or to the back of the figure plane. Blue squares are Cu^{2+} ions, and the purple tetrahedrons show P ions.

ions in the Néel state can be obtained by the $^{63,65}\text{Cu}$ NMR spectrum in zero external field (ZFNMR).

The spectrum, recorded at a liquid-He temperature of 4.2 K with the usual spin echo pulse sequence, is given in Fig. 13. The frequencies and the linewidths from fitting the spectrum by six Lorentzian lines are given in Table IV. Sharp resonance lines manifest equal fields around the copper ions in the sample. Both copper isotopes, ^{63}Cu and ^{65}Cu , have a nuclear spin $I = \frac{3}{2}$. The natural abundance of the ^{63}Cu isotope is about 2 times larger than that of the ^{65}Cu isotope; therefore, the lines in the spectrum can easily be recognized, as shown in Fig. 13. In the presence of strong local magnetic field B_{loc} created by the localized d electron the NMR spectrum of copper is due to three allowed transitions between quadrupolar split Zeeman energy levels: a central transition (between the energy levels $m = \pm\frac{1}{2} \longleftrightarrow \mp\frac{1}{2}$) and two satellite transitions (between the energy levels $m = -\frac{3}{2} \longleftrightarrow -\frac{1}{2}$ and $m = \frac{3}{2} \longleftrightarrow \frac{1}{2}$). Exact resonance frequencies can be calculated numerically by finding the eigenvalues of the Hamiltonian

TABLE III. Principal dipolar field projections at phosphorus ions of BaTCPO assuming the structure of Cu^{2+} magnetic moments $\Gamma_3(1)$ and $\Gamma_3(2)$ (given in Ref. [1]), compared with the experimentally determined values of B_{int} .

	$\Gamma_3(1)$	$\Gamma_3(2)$	Experiment
B_a	37.5 mT	42.2 mT	8.9 mT
B_b	90.1 mT	36.0 mT	31.2 mT
B_c	11.2 mT	0.75 mT	14.6 mT
Total	$B_{\text{dip}} = 97.7$ mT	$B_{\text{dip}} = 55.5$ mT	$B_{\text{int}} = 35.6$ mT

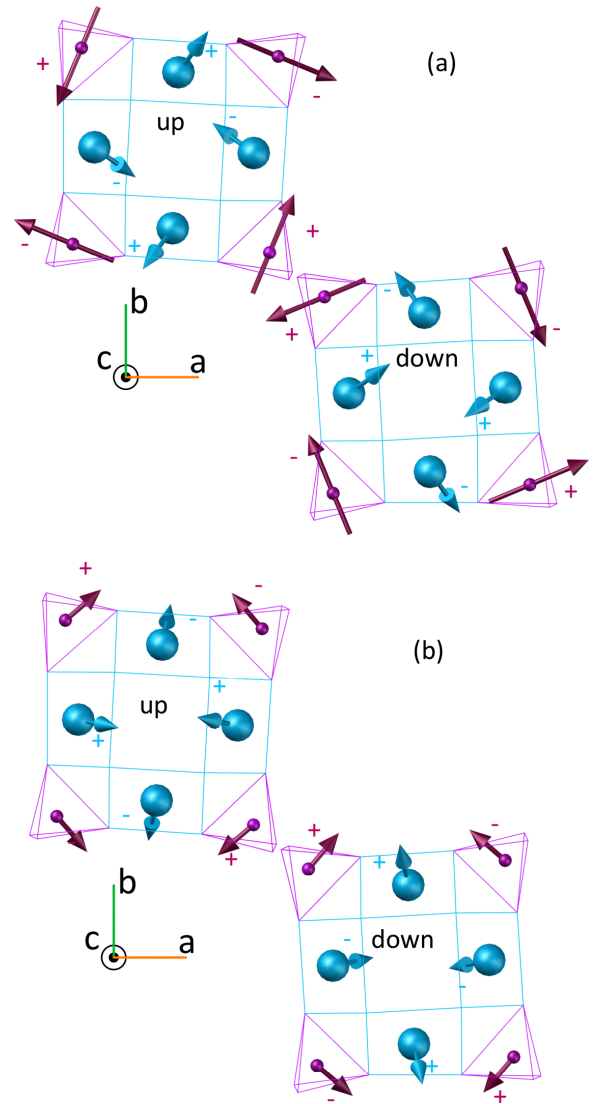


FIG. 12. Calculated dipolar field direction at phosphorus ions of the BaTCPO unit cell (a) assuming the structure of Cu^{2+} magnetic moments $\Gamma_3(1)$ (given in Ref. [1]) and (b) assuming the structure $\Gamma_3(2)$. The red arrows represent the dipole fields. The length of the arrows corresponds to the relative value of dipolar field in both cases and that in Fig. 11. Blue arrows represent directions of the Cu^{2+} magnetic moments and their sizes in the two cases.

which includes the Zeeman interaction term characterized by the Larmor frequency ν_L and the quadrupolar coupling term given by the quadrupolar frequency ν_Q , the asymmetry parameter of the electric field gradient (EFG) tensor η , and Euler angles α, β, γ , transforming the EFG tensor into the magnetic-field-oriented frame. We found an excellent match between observed frequencies and calculated frequencies (see Table IV) using the following parameters: $\nu_L = 166.692$ MHz, $\nu_Q = 31.657$ MHz for ^{63}Cu and $\nu_L = 178.567$ MHz, $\nu_Q = 29.290$ MHz for ^{65}Cu , with an axially symmetric EFG tensor $\eta = 0$, oriented with the main axis along the local magnetic field direction ($\beta = 0$, with arbitrary α and γ in the case of an axially symmetric EFG tensor). The Larmor frequencies of copper nuclei correspond to a local magnetic field at Cu

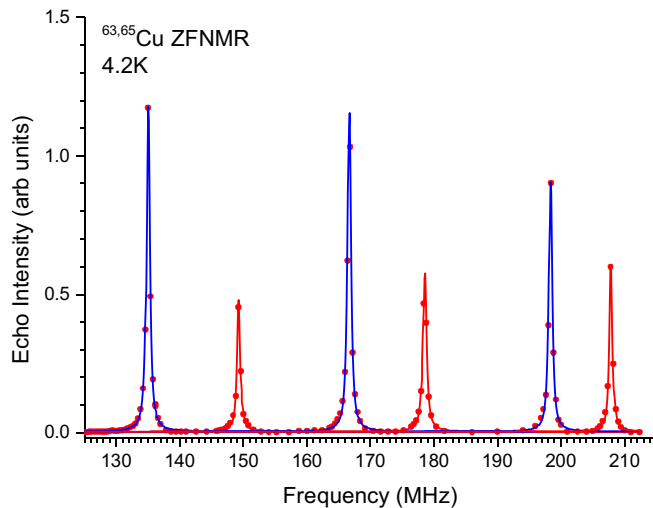


FIG. 13. $^{63,65}\text{Cu}$ ZFNMR spectrum of BaTCPO at 4.2 K. The blue lines correspond to the resonances of ^{63}Cu ; the red lines belong to ^{65}Cu resonances. Red dots are experimental echo amplitudes, and the solid lines are computer fits by Lorentzian lines.

ions of $B_{\text{loc}} = 14.77$ T. In the square cupola the copper nucleus is surrounded by four oxygen ions, forming a CuO_4 plane of a slightly distorted square. Such local symmetry of charges creates an axially symmetric lattice contribution to the EFG tensor where the main axis is perpendicular to the plane direction. The other contribution to the EFG tensor is caused by the hole in the $\text{Cu}^{2+}d$ shell. That contribution to the EFG tensor has symmetry similar to the lattice contribution, although with the opposite sign. Therefore, the main axis of the EFG tensor and the magnetic moment on copper in the square cupola compound must be perpendicular to the plane of CuO_4 plaquettes, which confirms the $\Gamma_3(2)$ magnetic structure as found already in neutron diffraction studies [1,6]. It is interesting to note that in antiferromagnetic CuO [18] the local field at copper is 12.15 T [19]. An overview of the EFG values at copper nuclei in oxides is given in Ref. [20].

IV. CONCLUSION

We performed ^{31}P NMR of the antiferromagnetic square cupola compound $\text{Ba}(\text{TiO})\text{Cu}_4(\text{PO}_4)_4$ in applied magnetic field $B = 4.7$ T and provided an in-depth overview of the local magnetic environment around the Cu^{2+} cupolas. From

TABLE IV. Observed and calculated resonance frequencies and the full linewidths at half height (FWHH) in the $^{63,65}\text{Cu}$ ZFNMR spectrum.

Nucleus	Transition	Frequency (MHz)		FWHH (MHz)
		Observed	Calculated	
^{63}Cu	$-\frac{3}{2} \longleftrightarrow -\frac{1}{2}$	198.355(5)	198.349	0.61
	$-\frac{1}{2} \longleftrightarrow \frac{1}{2}$	166.686(3)	166.692	0.62
	$\frac{1}{2} \longleftrightarrow \frac{3}{2}$	135.042(4)	135.035	0.61
^{65}Cu	$-\frac{3}{2} \longleftrightarrow -\frac{1}{2}$	207.857(8)	207.857	0.56
	$-\frac{1}{2} \longleftrightarrow \frac{1}{2}$	178.569(5)	178.568	0.67
	$\frac{1}{2} \longleftrightarrow \frac{3}{2}$	149.278(9)	149.278	0.59

the ^{31}P NMR frequency dependence of the single-crystal orientation we successfully determined the principal values of the ^{31}P magnetic shift tensor and the orientation of eight magnetic tensors in the unit cell at room temperature and at temperature $T = 6$ K. The Knight shift temperature dependence enabled us to determine the hyperfine field on ^{31}P nuclei $H_{\text{hf}} = 7.65(5)$ kOe/ μ_B for $a\parallel B$ and $H_{\text{hf}} = 7.40(5)$ kOe/ μ_B for $c\parallel B$. The temperature dependence of ^{31}P spin-lattice relaxation resulted in an approximation of the exchange interaction constant between Cu^{2+} ions of $J = 12$ K. The ^{31}P NMR frequency dependence on the single-crystal orientation in the antiferromagnetic state gave a clear picture of local magnetic fields at ^{31}P ions. The static magnetic field at every phosphorus was determined as $B_{\text{int}} = 35.6$ mT. The experimental configuration of the local field was compared to the calculated dipolar field for several magnetic arrangements of the copper magnetic moments. The NMR spectrum of $^{63,65}\text{Cu}$ in a magnetically ordered state at zero external field allowed us to unambiguously determine the size of $B_{\text{loc}} = 14.77$ T and the direction of the localized magnetic moment to be perpendicular to the plane of the CuO_4 plaquette, which confirms the $\Gamma_3(2)$ magnetic structure, as determined previously in neutron diffraction studies [1,6].

ACKNOWLEDGMENTS

This research was supported by Estonian Research Council Grants No. IUT23-7 and No. PRG4, European Regional Development Fund Grant No. TK134, JSPS KAKENHI Grants No. JP17H01143, No. JP19H05823, and No. JP19H01847, and the MEXT Leading Initiative for Excellent Young Researchers (LEADER).

- [1] K. Kimura, P. Babkevich, M. Sera, M. Toyoda, K. Yamauchi, G. S. Tucker, J. Martius, T. Fennell, P. Manuel, D. D. Khalyavin, R. D. Johnson, T. Nakano, Y. Nozue, H. M. Rønnow, and T. Kimura, *Nat. Commun.* **7**, 13039 (2016).
- [2] K. Kimura, M. Toyoda, P. Babkevich, K. Yamauchi, M. Sera, V. Nassif, H. M. Rønnow, and T. Kimura, *Phys. Rev. B* **97**, 134418 (2018).
- [3] Y. Kato, K. Kimura, A. Miyake, M. Tokunaga, A. Matsuo, K. Kindo, M. Akaki, M. Hagiwara, S. Kimura, T. Kimura, and Y. Motome, *Phys. Rev. B* **99**, 024415 (2019).
- [4] K. Kimura, Y. Kato, K. Yamauchi, A. Miyake, M. Tokunaga, A. Matsuo, K. Kindo, M. Akaki, M. Hagiwara, S. Kimura, M. Toyoda, Y. Motome, and T. Kimura, *Phys. Rev. Mater.* **2**, 104415 (2018).
- [5] K. Kimura, S. Kimura, and T. Kimura, *J. Phys. Soc. Jpn.* **88**, 093707 (2019).
- [6] P. Babkevich, L. Testa, K. Kimura, T. Kimura, G. S. Tucker, B. Roessli, and H. M. Rønnow, *Phys. Rev. B* **96**, 214436 (2017).
- [7] S. S. Islam, K. M. Ranjith, M. Baenitz, Y. Skourski, A. A. Tsirlin, and R. Nath, *Phys. Rev. B* **97**, 174432 (2018).

- [8] V. Kumar, A. Shahee, S. Kundu, M. Baenitz, and A. V. Mahajan, *J. Magn. Magn. Mater.* **492**, 165600 (2019).
- [9] K. Kimura, M. Sera, and T. Kimura, *Inorg. Chem.* **55**, 1002 (2016).
- [10] J. R. Singer, *Phys. Rev.* **121**, 1357 (1961).
- [11] A. M. Clogston and V. Jaccarino, *Phys. Rev.* **104**, 929 (1956).
- [12] R. Nath, Y. Furukawa, F. Borsa, E. E. Kaul, M. Baenitz, C. Geibel, and D. C. Johnston, *Phys. Rev. B* **80**, 214430 (2009).
- [13] D. Arčon, I. Heinmaa, and R. Stern, in *Modern Methods in Solid-State NMR: A Practitioner's Guide*, edited by P. Hodgkinson, New Developments in NMR Vol. 15 (Royal Society of Chemistry, Cambridge, 2018), pp. 231–261.
- [14] M. Mehring, *Principles of High Resolution NMR in Solids, 2nd edition*, (Springer, Berlin Heidelberg, 1983).
- [15] EASYSYSPIN, easyspin.org, was used for rotations and Euler angles.
- [16] T. Moriya, *Prog. Theor. Phys.* **16**, 23 (1956); *J. Phys. Soc. Jpn.* **18**, 516 (1963).
- [17] A. Lombardi, M. Mali, J. Roos, and D. Brinkmann, *Phys. Rev. B* **53**, 14268 (1996).
- [18] T. Kimura, Y. Sekio, H. Nakamura, T. Siegrist, and A. P. Ramirez, *Nat. Mater.* **7**, 291 (2008).
- [19] T. Tsuda, T. Shimizu, H. Yasuoka, K. Kishio, and K. Kitazawa, *J. Phys. Soc. Jpn.* **57**, 2908 (1988).
- [20] T. Shimizu, *J. Phys. Soc. Jpn.* **62**, 772 (1993).

Correction: A conversion error caused a few errant symbols to appear after certain compounds; the error has been fixed and the misprints removed.